

Gaskinetic Solutions for High Knudsen Number Planar Jet Impingement Flows

Chunpei Cai* and Chun Zou

Department of Mechanical and Aerospace Engineering, New Mexico State University, Las Cruces, New Mexico, 88003, USA.

Received 4 August 2012; Accepted (in revised version) 28 November 2012

Communicated by Boo-Cheong Khoo

Available online 19 March 2013

Abstract. This paper presents a gaskinetic study and analytical results on high speed rarefied gas flows from a planar exit. The beginning of this paper reviews the results for planar free jet expanding into a vacuum, followed by an investigation of jet impingement on normally set plates with either a diffuse or a specular surface. Presented results include exact solutions for flowfield and surface properties. Numerical simulations with the direct simulation Monte Carlo method were performed to validate these analytical results, and good agreement with this is obtained for flows at high Knudsen numbers. These highly rarefied jet and jet impingement results can provide references for real jet and jet impingement flows.

PACS: 98.58.Fd, 47.45.Ab, 52.25.Fi, 52.55.Fa, 52.35.Py

Key words: Gaskinetic theory, jet, jet impingement, Monte Carlo method.

1 Introduction

Gaseous jets expanding into a vacuum and jet impingement on a normally set plate are two fundamental fluid dynamic problems with numerous applications in engineering, physics, chemistry and other disciplines. As the counterpart to the continuum flow situation, highly rarefied jet and jet impingement flows provide one bounding limit with insights to many problems by solely including molecular movement. In many applications, the contribution from particle collisions is insignificant. One important application is the atomic/molecular beam [1, 2] which is a crucial tool that leads to many extremely important scientific discoveries. Other important applications include materials processing inside vacuum chambers [3] and rocket plume effects in aerospace engineering [4, 5].

*Corresponding author. *Email addresses:* ccai@nmsu.edu (C. Cai), chun.zou@gmail.com (C. Zou)

As the most important signature, rocket plume is widely used for inferred radar detections and performance evaluations. Due to the importance, many communities have been investigating rarefied gaseous jet and jet impingement flows for decades.

This paper presents some solutions for highly rarefied, or collisionless, planar jet and jet impingement flows. Section 2 reviews some background; Section 3 presents the exact solutions for the problem of high Knudsen number planar free jet into a vacuum; Section 4 shows the exact solutions for rarefied two dimensional jet impingement on a normally set flat plate with a diffuse surface; Section 5 reports some exact solutions for planar rarefied gaseous jet impingement on a specular flat plate; and Section 6 includes comparisons of the exact analytical solutions and direct simulation Monte Carlo (DSMC) [6] simulation results of rarefied impingement flows. The last section summarizes this paper with a few conclusions.

2 Background

Compressible flows can usually be summarized into four categories by the definition of the Knudsen number (Kn), which is related with the Mach (Ma) and Reynolds (Re) numbers [6–8]:

$$Kn = \frac{\lambda_0}{L} = \frac{1}{\sqrt{2\pi}d^2n_0L} \sim \frac{Ma}{Re}, \quad (2.1)$$

where λ_0 is the molecular mean free path, L is a characteristic length, d is the molecular diameter, and n_0 is the gas number density at the nozzle exit. These four regimes are: continuum ($0 < Kn < 0.01$), velocity slip and temperature jump ($0.01 < Kn < 0.1$), transitional ($0.1 < Kn < 10$), and free molecular (or collisionless) ($10 < Kn$). This paper discusses two flows in the free molecular regime, we choose the duct width as the characteristic length L . For the numerical validations at the end of this paper, we choose $Kn = 100$ and use Eq. (2.1) to determine the number density n_0 at the nozzle exit.

This paper focuses on exact solutions for the problems of rarefied planar jet expanding into a vacuum and jet impingement on a normally set plate with a diffused or a specular surface. A diffused reflection occurs when a particle collides at a surface, and it bounces back reversely and uniformly inside the solid angle on the other side of the local tangent plane. For a planar plate surface, the solid angle forms a span of π . For a specular reflection case, the reflected particle's normal momentum is reversed while the tangent momentum maintains unchanged.

For rarefied jet and jet impingement flows, there are many studies based on continuum theories, for example, the Navier-Stokes equations, boundary layer theory, characteristic lines, and Prandtl-Meyer flows [9]. For the high Knudsen number regime, there are many numerical and experimental studies and reports for the complete flowfield and surface properties. Most of the past studies adopted some simplifications. Noller [10] proposed a solid angle treatment to consider the nozzle exit geometry and obtained the plume density field expressed with integrations over the solid angle. Kogan [11] dis-

cussed two free molecular flows, over a convex wall or out of a nozzle. His discussions considered the effects from the speed ratio and angle of attack; however, the detailed geometry factors are not included at all. For jet and jet impingement flows, the geometry factors, such as the nozzle width and the distance from the nozzle center to the plate center, are more complex than the speed ratio factor. Narasimha [12] discussed the problem of a collisionless effusion flow through a circular hole between two chambers of different pressure. The average gas velocity at the two chamber ends is assumed to be zero. For the case of free molecular flows out of a planar exit with a nonzero average velocity, Narasimha's investigation [13] indicated that the plume solution is rather complicated involving many cosine functions. Another rocket plume treatment, which is also based on collisionless flows, was suggested by Woronowicz [14]. This treatment splits the exit into many small segments; as such, the unsteady density and pressure distributions in the flowfield can be computed numerically. Further, the concept of starting surface was proposed and alleviates the difficulty of the problem.

Recently, an approach [15–18] to study rarefied free jet into a vacuum was suggested and applied. It provided two sets of detailed solutions for rarefied planar and circular plume flows. These plume solutions only considered collisionless flow situations, such as plasma flows fire from an electric propulsion device. The collision effects were completely neglected. A recent validation work on this set of gaskinetic solutions extend the solutions for highly rarefied round jet into a vacuum to the near-continuum regime [19]. The conclusions are:

1. Even though the set of formulae were derived for collisionless flows, they are applicable for transitional and near continuum flow regimes as well, due to the fact that at high speed, molecules have less time to diffuse normally from the main flow direction. We can also equivalently use the relation among the Knudsen, Mach and Reynolds numbers, Eq. (2.1). This relation indicates, for a fixed Reynolds number, a high Mach number actually ensures a high Knudsen number.
2. The gaskinetic solutions for highly rarefied plume flow provide complete and accurate flowfields of density, velocity and pressure, with complex factors of speed ratio and geometry factors. By comparison, the widely used cosine law or the Simons plume model [20] provides density fields only with a simple cosine function; and Kogan's results did not include the important geometry factors.
3. Even for density, the gaskinetic solutions are more accurate than the Simons plume model.

As the counterpart to the problems of round jet and jet impingement flows, [21] we expect that the problems of rarefied planar jet and jet impingement can provide us new insights. This paper summarizes the past solutions for rarefied free planar jet into a vacuum, in the following section. Based on these solutions, we can extend the results to planar jet impingement problems.

In this paper, subscripts "0", "1", "2", "3" represent properties at nozzle exit, a flow-field point for the problem of free jet, and impingement on a plate of diffuse or specular reflections, respectively.

3 Analytical solutions for rarefied planar jet into a vacuum

For a dilute equilibrium gas flow with a zero average macroscopic velocity, it is reasonable to assume the velocity distribution is Maxwellian [6,7,22]. With a number density n_0 and a temperature T_0 , the thermal velocity distribution function is:

$$f(u,v,w) = n_0 \left(\frac{\beta_0}{\pi} \right)^{\frac{3}{2}} \exp(-\beta_0(u^2 + v^2 + w^2)), \quad (3.1)$$

where $\beta_0 = \frac{1}{2RT_0}$. The highest velocity probability occurs at the origin point. For a flow with a nonzero average value of U_0 along the X direction but a zero value along the Y direction, the integration domain for a flowfield point maintains the same shape but shifts left along the u -axis by U_0 .

With a known velocity distribution $f(u,v,w)$ at a point (X,Y,Z) , the macroscopic average number density, velocity components, temperature and pressure can be evaluated using the velocity distribution function [7]:

$$n(X,Y,Z) = \int_{\Omega} f(u,v,w) du dv dw, \quad (3.2a)$$

$$U(X,Y,Z) = \frac{1}{n(X,Y,Z)} \int_{\Omega} u f(u,v,w) du dv dw, \quad (3.2b)$$

$$V(X,Y,Z) = \frac{1}{n(X,Y,Z)} \int_{\Omega} v f(u,v,w) du dv dw, \quad (3.2c)$$

$$T(X,Y,Z) = \frac{1}{3Rn(X,Y,Z)} \int_{\Omega} (C_1^2 + C_2^2 + C_3^2) f du dv dw, \quad (3.2d)$$

$$P(X,Y,Z) = n(X,Y,Z)kT(X,Y,Z), \quad (3.2e)$$

where k is the Boltzmann constant, and Ω represents the integral domain in the thermal velocity space [16].

Recently, a gaskinetic approach with a velocity-location relation was proposed and applied to obtain the exact solutions for planar rarefied jet into a vacuum [16]:

$$\frac{X}{u+U_0} = \frac{Y-y}{v}. \quad (3.3)$$

With this approach and relation, it is possible to obtain exact solutions for several highly rarefied flows [16,19,23]. The key relation of velocity-location is as follows: from a specific point (x,y) at the exit, only particles with specific velocity components can arrive at a specific point $P(X,Y)$ in front of the exit. This equation guarantees a one-to-one mapping

relation between velocities and locations, provides boundaries for the integral domain, and simplifies the integration process by changing integral variables. For a planar situation:

$$\tan(\theta) = \frac{Y-y}{X} = \frac{v}{u+U_0}, \quad -H < y < H, \quad (3.4a)$$

$$\tan(\theta_1) = \frac{Y-H}{X}, \quad \tan(\theta_2) = \frac{Y+H}{X}, \quad (3.4b)$$

where H is the semi-height of a planar exit. To simplify the results, we define $A(x) = 1 + \operatorname{erf}(S_0 \cos(x))$, and $S_0 = U_0 \sqrt{\beta_0}$ as the exit speed ratio; the free jet flow field results are:

$$\begin{aligned} \frac{n_1(X,Y)}{n_0} &= \frac{\theta_2 - \theta_1}{2\pi} \exp(-S_0^2) + \frac{1}{4} [\operatorname{erf}(S_0 \sin \theta_2) - \operatorname{erf}(S_0 \sin \theta_1)] \\ &\quad + \frac{S_0}{2\sqrt{\pi}} \int_{\theta_1}^{\theta_2} \exp(-S_0^2 \sin^2 \theta) \cos \theta \operatorname{erf}(S_0 \cos \theta) d\theta, \end{aligned} \quad (3.5a)$$

$$\begin{aligned} \frac{U_1(X,Y)}{\sqrt{2RT_0}} &= \frac{1}{2\pi} \frac{n_0}{n_1} \exp(-S_0^2) \left\{ \frac{1}{2} S_0 (\theta_2 - \theta_1) + \frac{1}{4} S_0 [\sin(2\theta_2) - \sin(2\theta_1)] \right. \\ &\quad \left. + \frac{\sqrt{\pi}}{2} \int_{\theta_1}^{\theta_2} (1 + 2S_0^2 \cos^2 \theta) \cos \theta \exp(S_0^2 \cos^2 \theta) A(\theta) d\theta \right\}, \end{aligned} \quad (3.5b)$$

$$\frac{V_1(X,Y)}{\sqrt{2RT_0}} = \frac{1}{4\sqrt{\pi}} \frac{n_0}{n_1} \left\{ \exp(-S_0^2 \sin^2 \theta_1) \cos \theta_1 A(\theta_1) - \exp(-S_0^2 \sin^2 \theta_2) \cos \theta_2 A(\theta_2) \right\}, \quad (3.5c)$$

$$\begin{aligned} \frac{T_1(X,Y)}{T_0} &= \frac{1}{6\pi} \frac{n_0}{n_1} \exp(-S_0^2) \left\{ (3 + S_0^2) (\theta_2 - \theta_1) + \frac{S_0^2}{2} [\sin(2\theta_2) - \sin(2\theta_1)] \right. \\ &\quad \left. + 2\sqrt{\pi} \int_{\theta_1}^{\theta_2} (2 + S_0^2 \cos^2 \theta) S_0 \cos \theta \exp(S_0^2 \cos^2 \theta) A(\theta) d\theta \right\} - \frac{U_1^2 + V_1^2}{3RT_0}, \end{aligned} \quad (3.5d)$$

$$P_1(X,Y) = n_1(X,Y) k T_1(X,Y). \quad (3.5e)$$

The free jet center line results are:

$$\theta_1 = -\theta_2, \quad \tan \theta_2 = \frac{H}{X}, \quad (3.6a)$$

$$\begin{aligned} \frac{n_1(X,0)}{n_0} &= \frac{\theta_2}{\pi} \exp(-S_0^2) + \frac{1}{2} \operatorname{erf}(S_0 \sin \theta_2) \\ &\quad + \frac{S_0}{\sqrt{\pi}} \int_0^{\theta_2} \exp(-S_0^2 \sin^2 \theta) \cos \theta \operatorname{erf}(S_0 \cos \theta) d\theta, \end{aligned} \quad (3.6b)$$

$$\begin{aligned} \frac{U_1(X,0)}{\sqrt{2RT_0}} &= \frac{1}{2\pi} \frac{n_0}{n_1} \exp(-S_0^2) \left\{ S_0 \theta_2 + \frac{S_0}{2} \sin(2\theta_2) \right. \\ &\quad \left. + \sqrt{\pi} \int_0^{\theta_2} (1 + 2S_0^2 \cos^2 \theta) \cos \theta \exp(S_0^2 \cos^2 \theta) A(\theta) d\theta \right\}, \end{aligned} \quad (3.6c)$$

$$\frac{T_1(X,0)}{T_0} = \frac{-U_1^2}{3RT_0} + \frac{1}{6\pi} \frac{n_0}{n_1} \exp(-S_0^2) \left\{ (6+2S_0^2)\theta_2 + S_0^2 \sin(2\theta_2) + 4\sqrt{\pi} \int_0^{\theta_2} (2+S_0^2 \cos^2 \theta) S_0 \cos \theta \exp(S_0^2 \cos^2 \theta) A(\theta) d\theta \right\}. \quad (3.6d)$$

This set of solutions include two types of factors: geometry factors represented by θ_1 and θ_2 and complex nonlinear relations with normalized average exit velocity, S_0 .

There are asymptotes for the centerline velocity and temperature:

$$\lim_{X \rightarrow \infty} \frac{U_1(X,0)}{\sqrt{2RT_0}} = \frac{\pi \exp(-S_0^2) \{ S_0 + \sqrt{\pi} (\frac{1}{2} + S_0^2 \exp(S_0^2)) \}}{\exp(-S_0^2) + \sqrt{\pi} S_0}, \quad (3.7a)$$

$$\lim_{X \rightarrow \infty} \frac{T_1(X,0)}{T_0} = \frac{3 + 2S_0^2 + 2\sqrt{\pi} S_0 \exp(S_0^2) (2 + S_0^2)}{\exp(-S_0^2) + \sqrt{\pi} S_0}. \quad (3.7b)$$

4 High Knudsen number jet impingement on a normally set flat diffuse plate

This section presents solutions for rarefied jet impingement on a flat diffusive plate, as an extension from the problem of rarefied jet into a vacuum.

Figs. 1 and 2 illustrate the problem of impingement flow with diffuse reflections and the corresponding velocity phase. For a high speed gaseous jet into a vacuum from a nozzle with width $2H$, the flow at the exit is characterized by a number density n_0 and a temperature T_0 . At any point in front of the nozzle, the velocity phase consists of two groups of particles, one group from the nozzle and the other from the diffused flat plate.

This set of solutions are closely related to those for free jet flows. For example, there

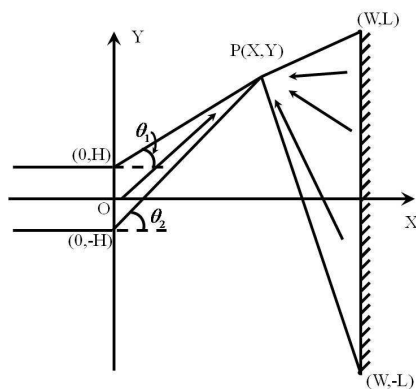


Figure 1: Illustration for the problem of jet impingement on a flat plate with diffuse reflections.

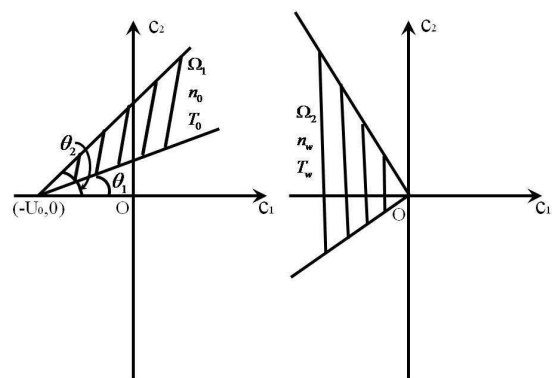


Figure 2: Thermal velocity phases for the problem of jet impingement on a flat plate with diffuse reflections.

are two parts in the number density at the plate surface:

$$n_2(L, Y) = n_1(L, Y) + n'_w(Y). \quad (4.1)$$

On the right hand side, $n'_w(Y)$ is the density factor contributed from the plate surface, and $n_1(L, Y)$ is the jet solution directly evaluated from Eq. (3.5a). It can be assumed that the group of reflected particles at the wall follow a special Maxwellian velocity distribution:

$$f_w(Y) = n_w(Y) \frac{\beta_w}{\pi} \exp[-\beta_w(c_1^2 + c_2^2)]. \quad (4.2)$$

An integration over u as a moment yields the flux relation at the wall:

$$n_1(L, Y)U_1(L, Y) = \frac{n_w \sqrt{RT_w}}{\sqrt{2\pi}}. \quad (4.3)$$

The slip velocity at the plate is:

$$V_2(L, Y) = \frac{\sqrt{RT_w}V_1(L, Y)}{\sqrt{RT_w} + \sqrt{\pi/2}U_1(L, Y)}. \quad (4.4)$$

On the plate, the temperature component is along the X -direction. The normal is defined along the X -direction.

$$\frac{T_2(L, Y)}{T_0} = \frac{n_w T_w}{2n_2(L, Y)T_0} + \frac{n_0 \exp(-S_0^2)}{2\pi n_2(L, Y)} \int_{\theta_1}^{\theta_2} \cos^2 \theta \left\{ 2 + 2S_0^2 \cos^2 \theta + \sqrt{\pi} S_0 \cos \theta (3 + 2S_0^2 \cos^2 \theta) \exp(S_0^2 \cos^2 \theta) A(\theta) \right\} d\theta, \quad (4.5a)$$

$$P_2(L, Y) = n_2(L, Y)kT_2(L, Y). \quad (4.5b)$$

The pressure and shear stress coefficients along the wall surface are:

$$C_p = \frac{n_w T_w}{2n_0 T_0 S_0^2} + \frac{\exp(-S_0^2)}{2\pi S_0^2} \int_{\theta_1}^{\theta_2} \cos^2 \theta \left\{ 2(1 + S_0^2 \cos^2 \theta) + \sqrt{\pi} S_0 \cos \theta (3 + 2S_0^2 \cos^2 \theta) \exp(S_0^2 \cos^2 \theta) A(\theta) \right\} d\theta, \quad (4.6a)$$

$$C_f = \frac{1}{2\pi S_0^2} \left\{ (\cos^2 \theta_1 - \cos^2 \theta_2) \exp(-S_0^2) + \sqrt{\pi} S_0 \cos^3 \theta_1 \exp(-S_0^2 \sin^2 \theta_1) A(\theta_1) - \sqrt{\pi} S_0 \cos^3 \theta_2 \exp(-S_0^2 \sin^2 \theta_2) A(\theta_2) \right\}. \quad (4.6b)$$

The location with the maximum shear stress is of special interest, and an approximation for this location is:

$$\frac{y_{crit}}{D} = \sqrt{\frac{(L/D)^2}{3S_0^2} - \frac{1}{12}}, \quad (4.7)$$

this result is based on one assumption that the L/D is large. In one NASA dust experiment, it was found that the largest ground shear stress happens at a location proportional to L/D , while inversely proportional to the nozzle exit Mach number [24]. Eq. (4.7) provides a strong support for this result. The corresponding simplified maximum shear stress value is:

$$\frac{\tau_{\max}}{\rho_0 U_0^2 / 2} = \frac{1}{2\sqrt{3\pi}} [1 + \operatorname{erf}(S_0)] \left[1 + \frac{3}{2S_0^2} \right] \frac{D}{L}. \tag{4.8}$$

Heat flux on the plate surface is:

$$\begin{aligned} C_q = & \frac{\exp(-S_0^2)}{4\pi S_0^2} \left[\int_{\theta_1}^{\theta_2} \left\{ \frac{\sqrt{\pi}}{S_0} \left[\frac{3}{2} + 6S_0^2 \cos^2 \theta + 2S_0^4 \cos^4 \theta + \left(\frac{1}{2} + \beta_0 V_2^2 \right) (1 + 2S_0^2 \cos^2 \theta) \right] \right. \right. \\ & \times \exp(S_0^2 \cos^2 \theta) A(\theta) + \cos \theta (6 + 2S_0^2 \cos^2 \theta + 2\beta_0 V_2^2) \left. \right\} \cos \theta d\theta \\ & - \frac{V_2}{U_0} \int_{\theta_1}^{\theta_2} \sin(2\theta) \left\{ 2 + 2S_0^2 \cos^2 \theta \right. \\ & \left. \left. + \sqrt{\pi} \exp(S_0^2 \cos^2 \theta) A(\theta) (3S_0 \cos \theta + 2S_0^3 \cos^3 \theta) \right\} d\theta \right] - \frac{1 + \frac{\beta_w V_2^2}{2}}{\sqrt{\pi} S_0^3} \frac{n_w}{n_0}. \end{aligned} \tag{4.9}$$

The density field $n_2(X, Y)$ is:

$$n_2(X, Y) = n_1(X, Y) + \frac{L - X}{2\pi} \int_{-W}^W \frac{n_w(y_0) dy_0}{(Y - y_0)^2 + (X - L)^2}, \tag{4.10}$$

where the integral element is the contribution from the plate. If we define α as the slop for a line connecting point $P(X, Y)$ and a specific point (L, y_0) at the plate surface, the integration on α is transformed to an integration over y_0 , with another format of velocity-position relation:

$$\frac{u}{v} = \tan(\alpha) = \frac{X - L}{Y - y_0} \tag{4.11}$$

and

$$d\alpha = \frac{X - L}{(Y - y_0)^2 + (X - L)^2} dy_0. \tag{4.12}$$

The integration on y_0 ranges within a region $(-W, W)$, which can be either finite or infinite.

Similarly, other flow field solutions are as follows:

$$U_2(X, Y) = \frac{n_1}{n_2} U_1 - \frac{(L - X)^2}{4n_2 \sqrt{\pi \beta_w}} \int_{-W}^W \frac{n_w(y_0) dy_0}{[(Y - y_0)^2 + (X - L)^2]^{\frac{3}{2}}}, \tag{4.13a}$$

$$V_2(X, Y) = \frac{n_1}{n_2} V_1 + \frac{(L - X)}{4n_2 \sqrt{\pi \beta_w}} \int_{-W}^W \frac{n_w(y_0) (Y - y_0) dy_0}{[(Y - y_0)^2 + (X - L)^2]^{\frac{3}{2}}}, \tag{4.13b}$$

$$T_2(X,Y) = \frac{n_1}{n_2} T_1 + \frac{L-X}{2n_2\pi\beta_w} \int_{-W}^W \frac{n_w(y_0)dy_0}{(Y-y_0)^2 + (X-L)^2} - \frac{U_2^2 + V_2^2}{3R}, \tag{4.13c}$$

$$P_2(X,Y) = n_2(X,Y)kT_2(X,Y). \tag{4.13d}$$

5 High Knudsen number jet impingement on a normally set flat specular plate

A specular plate is the second limiting case for molecule reflections, corresponding to the diffuse reflection type. These two limiting cases bound all practical plate reflections, which are special combinations of completely specular and completely diffuse reflections. For specular reflections, a crucial requirement is to satisfy the zero flux along the normal direction of the wall, while the tangent direction velocity is unchanged. A slip velocity along the tangent direction is expected.

Fig. 3 illustrates this problem and an approach to solve this problem. An identical "virtual" nozzle is placed at the other side of the plate. The logic for this approach is the same as the continuum potential flow of a point source at one side of a flat plate. Fig. 4 shows the velocity phase for a general point $P(X,Y)$ between the nozzle and the plate. This velocity phase for the new nozzle has the same format of a general zero-centered Maxwellian distribution which is characterized by the same n_0 and T_0 . By following this approach, we can illustrate the particle's thermal velocity components related to the actual and virtual nozzles within one picture. Molecules from the true nozzle are confined inside the triangle with a vertex $(-U_0,0)$, and those particles reflected from the specular plate, i.e., the virtual nozzle, are confined within the other triangular domain with a vertex $(U_0,0)$.

With the same gaskinetic theory for the diffuse reflection case, and definitions for two

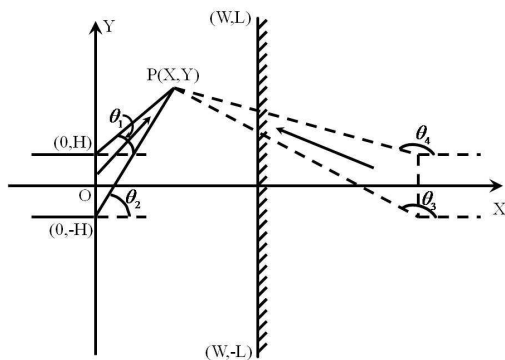


Figure 3: Illustration for the problem of jet impingement on a flat plate with specular reflections.

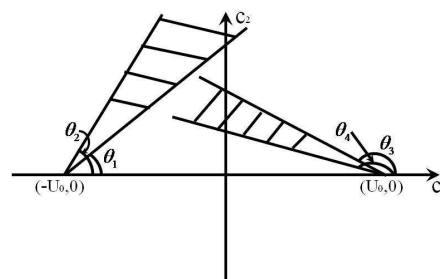


Figure 4: Thermal velocity phases for the problem of jet impingement on a flat plate with specular reflections.

new angles,

$$\theta_3 = \pi - \arctan \frac{Y+H}{2W-X}, \quad \theta_4 = \pi - \arctan \frac{Y-H}{2W-X}, \quad (5.1)$$

the following macroscopic properties can be obtained:

$$\begin{aligned} \frac{n_3(X,Y)}{n_0} = & \frac{\exp(-S_0^2)}{2\pi} (\theta_2 - \theta_1 + \theta_4 - \theta_3) + \frac{1}{4} \left[\operatorname{erf}(S_0 \sin \theta_2) - \operatorname{erf}(S_0 \sin \theta_1) + \operatorname{erf}(S_0 \sin \theta_4) \right. \\ & \left. - \operatorname{erf}(S_0 \sin \theta_3) \right] + \frac{S_0}{2\sqrt{\pi}} \left\{ \int_{\theta_1}^{\theta_2} \exp(-S_0^2 \sin^2 \theta) \cos \theta \operatorname{erf}(S_0 \cos \theta) d\theta \right. \\ & \left. + \int_{\theta_3}^{\theta_4} \exp(-S_0^2 \sin^2 \theta) \cos \theta \operatorname{erf}(S_0 \cos \theta) d\theta \right\}, \end{aligned} \quad (5.2a)$$

$$\begin{aligned} \frac{U_3(X,Y)}{\sqrt{2RT_0}} = & \frac{\exp(-S_0^2)}{2\pi} \frac{n_0}{n_3} \left\{ \frac{S_0}{2} (\theta_2 - \theta_1 + \theta_3 - \theta_4) + \frac{S_0}{4} [\sin(2\theta_2) - \sin(2\theta_1) + \sin(2\theta_3) \right. \\ & \left. - \sin(2\theta_4)] + \frac{\sqrt{\pi}}{2} \left[\int_{\theta_1}^{\theta_2} (1 + 2S_0^2 \cos^2 \theta) \cos \theta \exp(S_0^2 \cos^2 \theta) A(\theta) d\theta \right. \right. \\ & \left. \left. + \int_{\theta_3}^{\theta_4} (1 + 2S_0^2 \cos^2 \theta) \cos \theta \exp(S_0^2 \cos^2 \theta) [1 - \operatorname{erf}(S_0 \cos \theta)] d\theta \right] \right\}, \end{aligned} \quad (5.2b)$$

$$\begin{aligned} \frac{V_3(X,Y)}{\sqrt{2RT_0}} = & \frac{1}{4\sqrt{\pi}} \frac{n_0}{n_3(X,Y)} \left\{ \exp(-S_0^2 \sin^2 \theta_1) \cos \theta_1 A(\theta_1) - \exp(-S_0^2 \sin^2 \theta_2) \cos \theta_2 A(\theta_2) \right. \\ & \left. + \exp(-S_0^2 \sin^2 \theta_4) \cos \theta_4 [1 - \operatorname{erf}(S_0 \cos \theta_4)] \right. \\ & \left. - \exp(-S_0^2 \sin^2 \theta_3) \cos \theta_3 [1 - \operatorname{erf}(S_0 \cos \theta_3)] \right\}, \end{aligned} \quad (5.2c)$$

$$\begin{aligned} \frac{T_3(X,Y)}{T_0} = & \frac{\exp(-S_0^2)}{6\pi} \frac{n_0}{n_3} \left\{ \frac{S_0^2}{2} [\sin(2\theta_2) - \sin(2\theta_1) + \sin(2\theta_4) - \sin(2\theta_3)] + (3 + S_0^2) (\theta_2 - \theta_1 \right. \\ & \left. + \theta_4 - \theta_3) + 2\sqrt{\pi} \left[\int_{\theta_1}^{\theta_2} (2 + S_0^2 \cos^2 \theta) S_0 \cos \theta \exp(S_0^2 \cos^2 \theta) A(\theta) d\theta \right. \right. \\ & \left. \left. - \int_{\theta_3}^{\theta_4} (2 + S_0^2 \cos^2 \theta) S_0 \cos \theta \exp(S_0^2 \cos^2 \theta) [1 - \operatorname{erf}(S_0 \cos \theta)] d\theta \right] \right\} \\ & - \frac{U_3^2 + V_3^2}{3RT_0}, \end{aligned} \quad (5.2d)$$

$$P_3(X,Y) = n_3(X,Y) k T_3(X,Y). \quad (5.2e)$$

It is evident that the above solutions of density, velocity, temperature, and pressure results have two parts due to the real and virtual nozzles.

As to the plate properties, they simplify to concise formats due to the symmetry and $U_3=0$ condition. The density, slip velocity, temperature, and pressure at the plate are:

$$\frac{n_3(L,Y)}{n_0} = \frac{\exp(-S_0^2)}{\pi} (\theta_2 - \theta_1) + \frac{1}{2} [\operatorname{erf}(S_0 \sin \theta_2) - \operatorname{erf}(S_0 \sin \theta_1)]$$

$$+ \frac{S_0}{\sqrt{\pi}} \left[\int_{\theta_1}^{\theta_2} \exp(-S_0^2 \sin^2 \theta) \cos \theta \operatorname{erf}(S_0 \cos \theta) \right] d\theta, \quad (5.3a)$$

$$\frac{V_3(L, Y)}{\sqrt{2RT_0}} = \frac{n_0}{2\sqrt{\pi n_3}} \left\{ \exp(-S_0^2 \sin^2 \theta_1) \cos \theta_1 A(\theta_1) - \exp(-S_0^2 \sin^2 \theta_2) \cos \theta_2 A(\theta_2) \right\}, \quad (5.3b)$$

$$\begin{aligned} \frac{T_3(L, Y)}{T_0} = & \frac{\exp(-S_0^2)}{2\pi} \frac{n_0}{n_3(L, Y)} \left[\int_{\theta_1}^{\theta_2} \cos^2 \theta \left\{ 2(1 + S_0^2 \cos^2 \theta) \right. \right. \\ & + \sqrt{\pi} S_0 \cos \theta (3 + 2S_0^2 \cos^2 \theta) \exp(S_0^2 \cos^2 \theta) A(\theta) \left. \right\} d\theta + \int_{\theta_3}^{\theta_4} \cos^2 \theta \left\{ 2(1 + S_0^2 \cos^2 \theta) \right. \\ & \left. \left. - \sqrt{\pi} S_0 \cos \theta (3 + 2S_0^2 \cos^2 \theta) \exp(S_0^2 \cos^2 \theta) [1 - \operatorname{erf}(S_0 \cos \theta)] \right\} d\theta \right], \quad (5.3c) \end{aligned}$$

$$\begin{aligned} C_p = & \frac{\exp(-S_0^2)}{2\pi S_0^2} \left[\int_{\theta_1}^{\theta_2} \cos^2 \theta \left\{ 2(1 + S_0^2 \cos^2 \theta) \right. \right. \\ & + \sqrt{\pi} S_0 \cos \theta (3 + 2S_0^2 \cos^2 \theta) \exp(S_0^2 \cos^2 \theta) A(\theta) \left. \right\} d\theta + \int_{\theta_3}^{\theta_4} \cos^2 \theta \left\{ 2(1 + S_0^2 \cos^2 \theta) \right. \\ & \left. \left. - \sqrt{\pi} S_0 \cos \theta (3 + 2S_0^2 \cos^2 \theta) \exp(S_0^2 \cos^2 \theta) [1 - \operatorname{erf}(S_0 \cos \theta)] \right\} d\theta \right]. \quad (5.3d) \end{aligned}$$

Shear stress and heat flux on the plate are zero due to the symmetry condition:

$$\tau_w = q_w = 0. \quad (5.4)$$

Along the impingement flow center line, due to special geometry relations, the solutions further degenerate:

$$\theta_1 = -\theta_2, \quad \theta_4 = 2\pi - \theta_3, \quad (5.5a)$$

$$\tan \theta_2 = \frac{H}{X}, \quad \tan \theta_3 = \frac{H}{X - 2L}, \quad (5.5b)$$

$$\begin{aligned} \frac{n_3(X, 0)}{n_0} = & \frac{S_0}{\sqrt{\pi}} \left\{ \int_0^{\theta_2} \exp(-S_0^2 \sin^2 \theta) \cos \theta \operatorname{erf}(S_0 \cos \theta) d\theta \right. \\ & + \int_{\theta_3}^{\pi} \exp(-S_0^2 \sin^2 \theta) \cos \theta \operatorname{erf}(S_0 \cos \theta) d\theta \left. \right\} \\ & + \frac{\exp(-S_0^2)}{\pi} (\pi + \theta_2 - \theta_3) + \frac{1}{2} [\operatorname{erf}(S_0 \sin \theta_2) - \operatorname{erf}(S_0 \sin \theta_3)], \quad (5.5c) \end{aligned}$$

$$\begin{aligned} \frac{U_3(X, 0)}{\sqrt{2RT_0}} = & \frac{1}{2\pi} \frac{n_0}{n_3} \exp(-S_0^2) \left\{ S_0 (\theta_2 + \theta_3 - \pi) + \frac{1}{2} S_0 [\sin(2\theta_2) + \sin(2\theta_3)] \right. \\ & + \sqrt{\pi} \left[\int_0^{\theta_2} (1 + 2S_0^2 \cos^2 \theta) \cos \theta \exp(S_0^2 \cos^2 \theta) A(\theta) d\theta \right. \\ & \left. \left. + \int_{\theta_3}^{\pi} (1 + 2S_0^2 \cos^2 \theta) \cos \theta \exp(S_0^2 \cos^2 \theta) [1 - \operatorname{erf}(S_0 \cos \theta)] d\theta \right] \right\}, \quad (5.5d) \end{aligned}$$

$$\begin{aligned} \frac{T_3(X,0)}{T_0} = & \frac{1}{6\pi} \frac{n_0}{n_3} \exp(-S_0^2) \left\{ S_0^2 [\sin(2\theta_2) - \sin(2\theta_3)] + (6 + 2S_0^2)(\theta_2 - \theta_3 + \pi) \right. \\ & + 4\sqrt{\pi} \left[\int_0^{\theta_2} (2 + S_0^2 \cos^2 \theta) S_0 \cos \theta \exp(S_0^2 \cos^2 \theta) A(\theta) d\theta \right. \\ & \left. \left. - \int_{\theta_3}^{\pi} (2 + S_0^2 \cos^2 \theta) S_0 \cos \theta \exp(S_0^2 \cos^2 \theta) [1 - \operatorname{erf}(S_0 \cos \theta)] d\theta \right] \right\} - \frac{U_3^2}{3RT_0}. \quad (5.5e) \end{aligned}$$

6 Validations

Even though most of the above analytical solutions involve several integral terms that cannot be explicitly removed, numerical evaluations were convenient via a computer. Most simulations were performed with a special DSMC package, GRASP [25]. In simulations for the free jet problem, an inlet boundary was used to represent the nozzle which was located at the left bottom corner; a symmetric line at the domain bottom represents the jet centerline and vacuum boundaries for other sides. For the jet impingement problem, an extra diffused or specular wall replaced the right vacuum boundary at the right side of the simulation domain. For less rarefied situations, molecular collisions were simulated using the Variable Hard Sphere (VHS) model, and the No Time Counter (NTC) method was adopted for the simulations. The mesh was uniform with $\Delta x = \Delta y$ and $\Delta x/\lambda_0 = 1.0$, and the time step was $\Delta t/t_0 = 1.0$, where λ_0 and t_0 were the reference mean free path and reference collision time based on the exit properties for the $\text{Kn} = 100$ scenario. For different DSMC simulations, a simulation time of at least $10,000t_0$ was performed before actual sampling processes started.

6.1 Free jet expanding into a vacuum

The rarefied free jet into a vacuum problem is different from the Prandtl-Meyer flow where gas can expand around the duct lip. If the exit average velocity is, $U_0 = 0$, the boundary line between the flow field and a vacuum is a vertical line extending upward from the upper exit lip. When the average velocity U_0 increases, the boundary line levels down towards the plume center, though it still starts with the upper lip $(0, H)$. For the analytical solutions, an effective boundary line of $n/n_0 = 0.0001$ is introduced to represent the plume edge [16], and the comparisons were restricted to areas within this boundary.

From the previous validation work, we conclude that the analytical free plume solutions, e.g., number density, velocity and pressure fields, are accurate. This set of free molecular flow solutions have some advantages over the traditional plume solution, which usually only contains the density results. Because the solutions for the problem plume impingement on a flat surface rely on the ones for the free plume, a detailed validation on the impingement solutions can further support free plume solutions. Because of this, the next two subsections validate the solutions for the problems of jet impingement thoroughly.

6.2 High Knudsen number jet impingement on a diffuse flat plate

Figs. 5, 6 and 7 show density, and velocity contours from the exact solutions and DSMC simulations. The Knudsen number is 100, which represents a highly rarefied flow well, and the speed ratio $S_0=2.0$. For this test case, essentially identical agreement is observed, and strongly supports the analytical collisionless flow solutions. To check the Knudsen number effects on flow field results, Fig. 8 shows the density contours at $Kn = 0.01$ and 1.0. As we can see, the patterns eventually transform from the collisionless flow to a near continuum flow with a developing shock wave.

Fig. 9 shows the wall pressure distributions. This figure illustrates the rarefaction effect with a fixed speed ratio, $S_0 = 2.0$. A DSMC simulation was performed to validate the collisionless pressure results. In the collisionless flow case, faster particles are less impeded and there are more high kinetic energy particles reaching the plate surface without losing their kinetic energy. As a result, higher Knudsen number flows have steeper pressure distributions at the plate center region. For flows with denser gas, more collisions

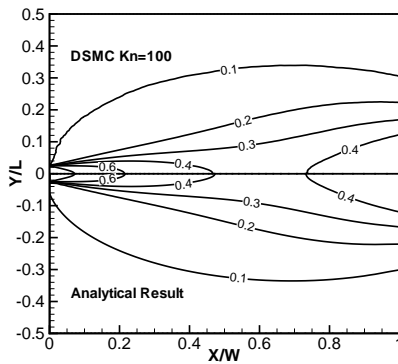


Figure 5: Diffuse plate: contours of normalized number density, collisionless flow, $S_0=2$.

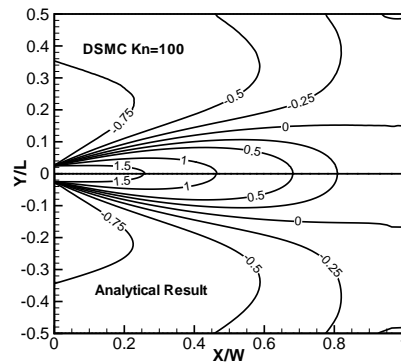


Figure 6: Diffuse plate: contours of normalized U -velocity, collisionless flow, $S_0=2$.

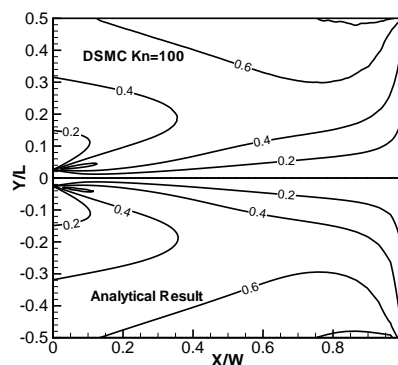


Figure 7: Diffuse plate: normalized V -velocity distribution, collisionless flow, $S_0=2$.

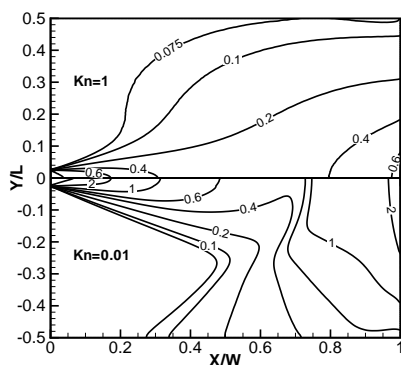


Figure 8: Diffuse plate: normalized number density distribution, low Kn number, $S_0=2$.

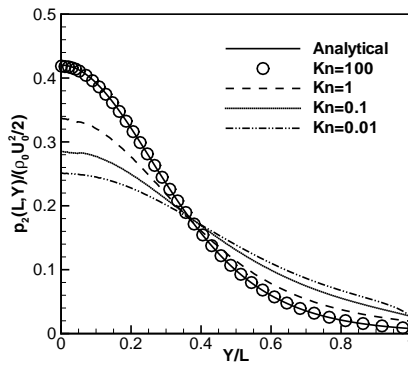


Figure 9: Diffuse plate: normalized pressure along the plate surface $P_{2w}(L,y)/(\rho_0 U_0^2/2)$, $S_0=2$.

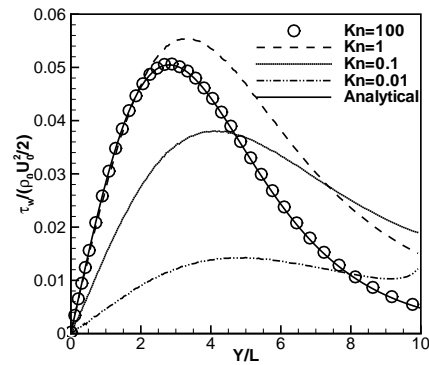


Figure 10: Diffuse plate: normalized shear stress along the plate surface with different Kn numbers, $\tau_{xy}(L,y)/(\rho_0 U_0^2/2)$, $S_0=2$.

reduce the incoming particles' kinetic energy and result in a relatively flatter pressure distribution curve.

Fig. 10 shows the rarefaction effects on the plate surface shear stress and the Knudsen numbers are different, but the speed ratios are the same. A group of DSMC simulation results of shear stress along the plate surface are used to validate the high Knudsen number exact solution, Eq. (4.6b). The comparison yields identical results. As the Kn number decreases, more frequent collisions scatter particles off the main flow direction and shift the highest shear stress point further off the center region. The highest shear stress coefficients and the corresponding places do not vary monotonically with the Kn numbers.

Fig. 11 shows the heat flux at the plate surface with different Knudsen numbers and the same speed ratio $S_0=2$. An exact analytical rarefied flow heat flux coefficient, Eq. (4.9), is plotted to compare the results. The agreement between the analytical and DSMC simulation results for the exact collisionless flow is fairly good. As the Kn number continues to decrease, the heat flux continues to drop because more frequent collisions scatter high speed molecules before they reach the plate.

Fig. 12 shows profiles of normalized slip velocity along a diffusive plate surface, $V(L,y)$, with the same $S_0=2$ but different Kn numbers. This picture illustrates that the slip velocity does not always decrease following the Knudsen numbers. This can be explained by the fact that there are two competing factors in the slip velocity expression of Eq. (4.4). The collisions affect them differently with varying Knudsen numbers.

Figs. 13 and 14 show the centerline number density and velocity for the diffuse plate surface scenario. At the exit, the density profiles increase due to the fact that faster molecules effuse from the exit, and this effect is larger than the reflected back particles. With the same reason, the centerline velocity increases as S_0 increases; at the plate center, all the centerline velocities must be zero to satisfy the non-penetration boundary condition.

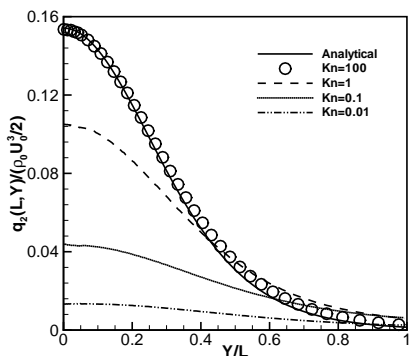


Figure 11: Diffuse plate: normalized heat flux $q_{2w}(L,y)/(\rho_0 U_0^3/2)$ along the plate surface, $S_0 = 2$, different Kn numbers.

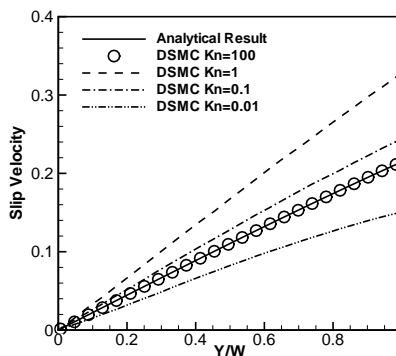


Figure 12: Diffuse plate: normalized slip velocity along the plate surface, $V(L,y)$, $S_0 = 2$.

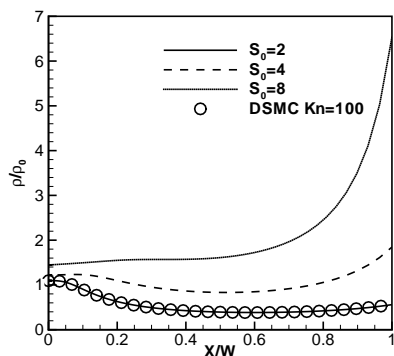


Figure 13: Diffuse plate: normalized plume centerline number density with different Kn numbers, $S_0 = 2$.

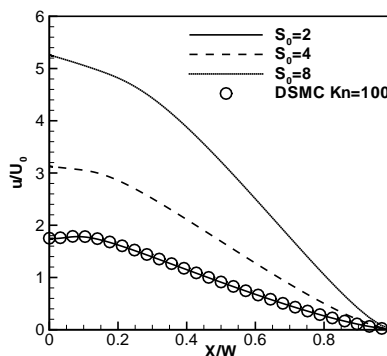


Figure 14: Diffuse plate: normalized plume centerline U -velocity with different speed ratios, $Kn = 100$.

6.3 Collisionless jet impingement on a flat specular plate

Fig. 15 compares analytical collisionless flow density results, Eq. (5.2a), and the corresponding results from DSMC simulations, $Kn = 100$ and $S_0 = 2$. Figs. 16 and 17 compare the corresponding velocity components. Fig. 18 shows comparison of exact analytical Eq. (5.2d) and DSMC simulation results of the temperature field. For these cases, the speed ratio is $S_0 = 2$ for the analytical and DSMC simulation results, while a Kn number of 100 is used for the DSMC simulation. These four figures yield the following conclusions:

1. The analytical and numerical simulation results are virtually identical, and this fact indicates results are correct for this specular reflection case;
2. Due to the virtual nozzle, the flow patterns are symmetric with $\partial()/\partial n = 0$ at the plate surface. By comparison, this pattern is not illustrated by the diffuse reflection case;

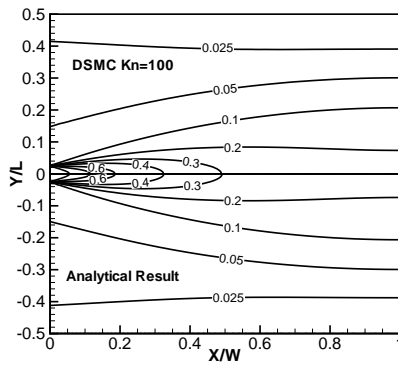


Figure 15: Specular plate: contours of normalized number density, $S_0 = 2$.

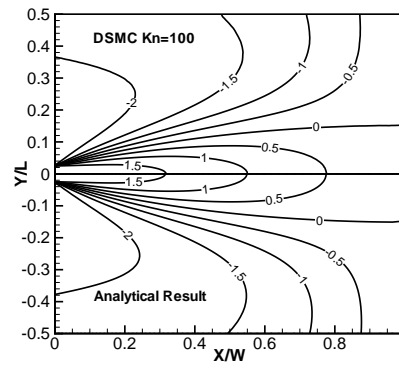


Figure 16: Specular plate: contours of normalized U -velocity component, $S_0 = 2$.

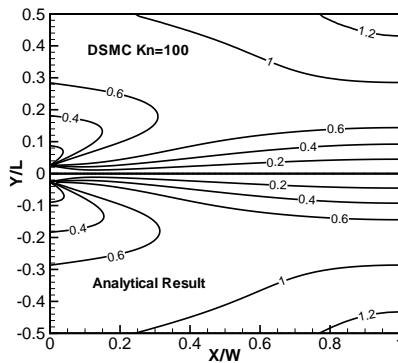


Figure 17: Specular plate: contours of normalized V -velocity component, $S_0 = 2$.

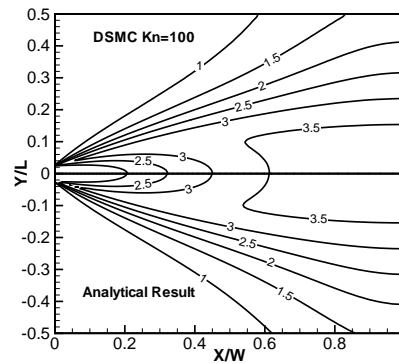


Figure 18: Specular plate: contours of normalized temperature, $S_0 = 2$.

3. The U -velocity at the plate is zero to satisfy the zero flux wall boundary condition;
4. At regions close to the plate, the temperature is high and irrelevant to the plate temperature. This is because at that region, there are two groups of molecules moving along opposite directions but the same speed. As a result, the velocity distribution function has a flatter span which means a higher temperature.

Figs. 19 and 20 show several pressure coefficient distributions along a specular reflective surface. The first one compares the rarefaction effect the exact analytical Eq. (5.3d) is presented and validated with a DSMC simulation, where the speed ratio is $S_0 = 2$. The pressure distribution at the plate center region achieves the maximum when the Kn number is the largest, i.e., collisionless flows. The other figure compares the speed ratio effects on the pressure results. If the gas is collisionless, then an increase of the speed ratio results in steeper and narrower pressure profiles because particles have high velocity and less time to diffuse along the direction normal to the jet flow direction.

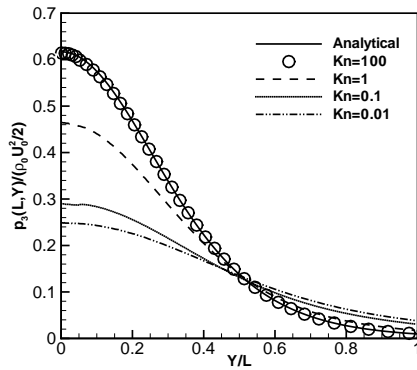


Figure 19: Specular plate: rarefaction effects on plate pressure distributions, $S_0 = 2$.

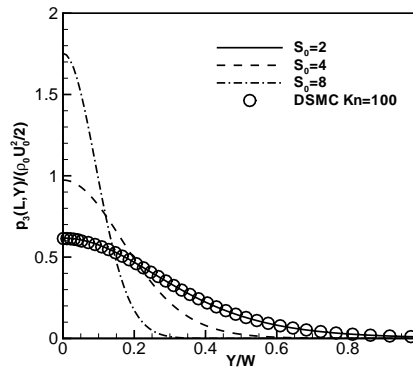


Figure 20: Specular plate: exit speed ratio effects on the plate pressure distributions.

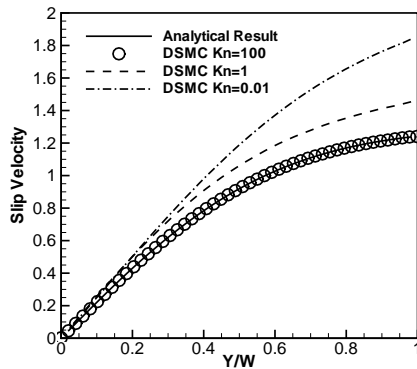


Figure 21: Specular plate: rarefaction effects on normalized plate slip velocity, $S_0 = 2$.

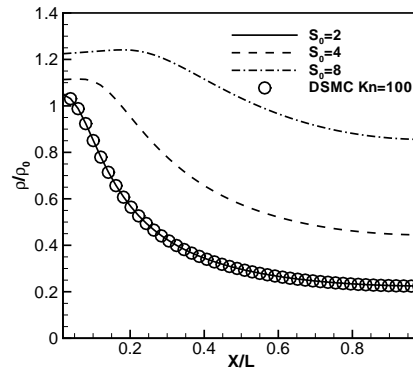


Figure 22: Specular plate: exit speed ratio effect on centerline density, $Kn = 100$.

Fig. 21 presents profiles of normalized slip velocity along a specular plate, with $S_0 = 2$ and different Kn numbers; the collisionless flow results are validated with a DSMC simulation. As the Kn number decreases, extra collisions actually push particles off the high density plate center. More particles with higher V -velocity component contribute to the slip velocity. This is the reason that the slip velocity increases with a decreasing Kn number. Different from diffuse plate slip velocity, Fig. 12 for the specular reflections, the slip velocity increases monotonically with lower Knudsen numbers, due to no extra contribution from the outer region to the plate center.

Fig. 22 shows profiles of centerline density for the case of a specular reflective flat plate with $Kn = 100$ but different S_0 . As the speed ratio increases, more molecules fire from the nozzle, resulting in higher density profiles. The $S_0 = 2$ profile is validated by DSMC simulation results. The density profile shifts up with S_0 , due to more incoming particles from the exit and more reflected particles from the plate.

7 Conclusions

This paper investigates collisionless planar jet impinging on a flat plate with either completely diffused or completely specular reflections. First, solutions for a planar free jet expanding into a vacuum are reviewed because they are the foundations for the impingement problem. An approach with a crucial velocity-location relation is used to solve these problems. Flowfield properties which include number density, velocity, temperature, and pressure formulae are presented for these problems. For the jet impingement problems, surface properties such as pressure coefficients, shear stress, heat flux, and slip velocity are included. Several DSMC simulations are performed to validate these analytical solutions, good or even essentially identical agreement is observed. To understand the rarefaction effects on the flows, several DSMC simulation results for different Knudsen number flows are also presented. When flows become near continuum, the departure from the exact solutions becomes more significant.

These final solutions are complex, and involve both geometry and speed ratio factors. The fundamental assumptions are the Maxwellian distributions at the nozzle exit and a velocity-locations relation. These solutions are the counterpart solutions for the continuum gaseous jet and jet impingement problems and provide us some insights to study these flows.

Acknowledgments

The work in this paper is partially sponsored from NSF-CBET-0854411, NSF-DMS-0914706 and NASA-ZTNMSU012209-DUST.

References

- [1] R. Campargue, Historical account and branching to rarefied gas dynamics of atomic & molecular beams: a continuing and fascinating odyssey commemorated by Nobel prizes awarded to 23 laureates in physics & chemistry, AIP Conference Proceeding, RGD24 International Symposium on Rarefied Gas Dynamics, Volume 762, Bari, Italy, July, 2005, pp. 32-46.
- [2] G. Sanna, and G. Tomassetti, Introduction to Molecular Beams Gas Dynamics, Imperial College Press, London, 2005.
- [3] R. Maev and V. Leshchynsky, Introduction to Low Pressure Gas Dynamic Spray, Wiley-Vch, Weinheim, 2008.
- [4] D. Hastings and H. Garrett, Spacecraft-Environment Interactions, Cambridge University Press, Cambridge, 1996.
- [5] P. Metzger and C. Immer, Jet-induced cratering of a granular surface with application to lunar spaceports, J. Aerosp. Eng., 22 (2009), 24.
- [6] G. Bird, Molecular Gas Dynamics and the Direct Simulation of Gas Flows, Oxford University Press, New York, 1994.

- [7] W. Vincenti and C. Kruger, *Introduction to Physical Gas Dynamics*, Krieger Publishing, Malabar, Florida, 1986.
- [8] G. Karniadakis, A. Beskok and N. Aluru, *Microflows and Nanoflows: Fundamentals and Simulation*, Springer, USA, 2005.
- [9] K. Naumann, The freezing of flow deflection in Prandtl-Meyer expansion to vacuum, RGD15 International Symposium on Rarefied Gas Dynamics, Grado, Italy, 2 (1988), pp. 524–533.
- [10] H. Noller, Approximate calculation of expansion of gas from nozzles into high vacuum, *J. Vac. Sci. Tech. A*, 3 (1966), 202.
- [11] M. Kogan, *Rarefied Gas Dynamics*, Plenum Press, New York, 1969.
- [12] R. Narasimha, Orifice flow of high Knudsen Number, *J. Fluid. Mech.*, 10 (1961), 371.
- [13] R. Narasimha, Collisionless expansion of gases into vacuum, *J. Fluid Mech.*, 12 (1962), 294.
- [14] M. Woronowicz, Proceedings of the 6th AIAA/ASME Joint Thermophysics and Heat Transfer Conference, Colorado Springs, CO, 20-23, 1994.
- [15] C. Cai, *Theoretical and Numerical Studies of Plume Flows in Vacuum Chambers*, VDM Publishing, Saarbrücken, Germany, 2011; also Ph.D. Dissertation, Dept. of Aerospace Engineering, University of Michigan, Ann Arbor, MI, 2005.
- [16] C. Cai and I. Boyd, Theoretical and numerical study of several free molecular flow problems, *J. Spacecr. Rockets*, 44 (2007), 619. DOI: 10.2514/1.25893.
- [17] C. Cai and I. Boyd, Collisionless gas flow expanding into vacuum, *J. Spacecr. Rockets*, 44 (2007), 1326. DOI: 10.2514/1.32173.
- [18] K. Khasawneh, H. Liu and C. Cai, Highly rarefied two-dimensional jet impingement on a flat plate, *Phys. Fluids*, 22 (2010), 1. doi:10.1063/1.3490409.
- [19] C. Cai and L. Wang, Numerical validations for a set of complete gaskinetic rocket plume solutions, *J. Spacecr. Rockets*, 41 (2012), 59. DOI:10.2514/1.A32046.
- [20] G. Simons, Effects of nozzle boundary layers on rocket exhaust plumes, *AIAA J.*, 10 (1972), 1534.
- [21] C. Cai and X. Huang, Rarefied circular jet impingement flows, *AIAA J.*, 50 (2012), 2908. DOI: 10.2514/1.J051785.
- [22] G. Gombosi, *Gaskinetic Theory*, Cambridge University Press, New York, 1994.
- [23] X. Chen, The impact force acting on a flat plate exposed normally to a rarefied plasma plume issuing from an annular or circular nozzle, *J. Phys. D Appl. Phys.*, 43 (2010), 315205.
- [24] N. Land and L. Clark, Experimental investigation of jet impingement on surfaces of fine particles in a vacuum environment, NASA-TN-D-2633, 1965.
- [25] H. Liu, C. Cai and C. Zou, An object-oriented implementation of the DSMC method, *Comput. Fluids*, 57 (2012), 65. DOI: 10.1016/j.compfluid.2011.12.007.